RSC Advances

PAPER

View Article Online
View Journal | View Issue

Cite this: *RSC Adv.*, 2015, **5**, 95038

TiO_2 nanofibers supported on Ti sheets prepared by hydrothermal corrosion: effect of the microstructure on their photochemical and photoelectrochemical properties†

Samiha Chaguetmi,[abc] Slimane Achour,[c] Ludovic Mouton,[b] Philippe Decorse,[b] Sophie Nowak,[b] Cyrille Costentin,[d] Fayna Mammeri[b] and Souad Ammar*[b]

Received 14th July 2015
Accepted 20th October 2015

DOI: 10.1039/c5ra13848e

www.rsc.org/advances

TiO_2/Ti nanostructures were synthesized by the hydrothermal route. Based on the operating conditions, namely the heating time and temperature, the microstructure of the produced titania was successfully varied from very thick and short nanofibers to very thin and long nanowires. UV-Visible diffuse reflectance spectroscopy also evidenced a net dependency of the optical properties of the produced semiconducting films, and consequently their photocatalytic and photoelectrocatalytic activity, to their synthesis conditions. Typically, the photodegradation of methylene blue in water under UV irradiation as well as the oxidation of water without additional bias were assessed and showed different efficiencies according the type of tested film.

Introduction

Due to its unique optical and electronic properties, titania, TiO_2, has been largely used for photocatalytic[1] degradation of organic pollutants in wastewater and photoelectrocatalytic[2] water splitting for hydrogen generation. Efforts in enhancing the photosensitivity of TiO_2 are still in progress and extensive research has been performed to optimize its crystalline structure, morphology and doping level to tentatively adapt its electronic structure and charge properties to the desired application.[3] It appears that among the three main crystalline titania polymorphs, the anatase phase exhibits the greatest photocatalytic activity, despite its metastability, while rutile, the most stable of the three, and brookite present only a modest and a zero activity, respectively.[4] It appears also that mixed phases, typically composites constituted by a large quantity of anatase and a small quantity of rutile, may exhibit a high photocatalytic response, which may exceed that of pure anatase.[3,5] Besides, among the tremendous explored TiO_2 morphologies, mainly based on differently sized and shaped nanostructures, 1D-morphologies, commonly nanorods, nanowires, nanofibers and nanotubes, seem to be the most suitable, thanks to their high surface area, small local electric field and band-gap tailoring flexibility.[6–12] Finally, the modification of TiO_2 host by metal and non-metal ions doping, oxygen stoichiometry change or sensitization with quantum dots have been widely investigated to extend UV photosensitivity of TiO_2 to visible light one, enhancing its wavelength light absorption range and then its sunlight energy conversion, overcoming its intrinsic limitation as a wide gap semiconductor.[13–16]

In this context, several chemical and physical routes have been developed to prepare tailored TiO_2 photocatalysts and photoelectrocatalysts. Among them those based on a hydrothermal treatment of bulk TiO_2 in an alkaline solution followed by a subsequent proton exchange and a moderate calcination in air appear to be well adapted to prepare anatase nanotubes[17,18] or nanowires.[18,20] As high are the alkaline concentration and reaction time and temperature as the nanowires are prevailingly obtained. Compared with nanotubes, nanowires are more stable at high temperature and in acid or alkaline solution,[19] making them more robust for a large environmental use. Routes based on a hydrothermal treatment of bulk Ti in alkaline and oxidative solution, followed by proton exchange and calcination in air, were also explored. They can be applied directly to cleaned Ti sheets[20] or to previously anodized ones.[21] They commonly provide more or less thin and long nanofibers. Focusing on this experimental approach, on the basis of our previous work,[22] we prepared a series of nanoscaled one-dimensional TiO_2 films supported on Ti sheets for which the reaction time and temperature were varied with a special

[a]*Faculté des Sciences, Université 20 Août 1955 de Skikda, Skikda, Algeria*

[b]*Interfaces Traitement Organisation et DYnamique des Systèmes, Université Paris Diderot, Sorbonne Paris Cité, CNRS UMR-7086, 15 rue Jean-Antoine de Baïf 75205, Paris, France. E-mail: ammarmer@univ-paris-diderot.fr; Fax: +33 1 5727 7263; Tel: +33 1 5727 8762*

[c]*National Polytechnic School of Constantine, Constantine, Algeria*

[d]*Laboratoire d'Electrochimie Moléculaire, Université Paris Diderot, Sorbonne Paris Cité, CNRS UMR-7591, Paris, France*

† Electronic supplementary information (ESI) available. See DOI: 10.1039/c5ra13848e

emphasis on the effect of these two experimental parameters on the structural, microstructural and electronic properties of the final products. The photocatalytic and photoelectrocatalytic behavior of all the produced samples were addressed by following the degradation of methylene blue in water and the oxidation of water at pH = 7, under mainly UV light irradiation, respectively.

Experimental

Film production

Titanium plate (0.5 mm thickness, 99.6% purity) was purchased from Goodfellow. Nanostructured titania was synthesized using a controlled hydrothermal corrosion of Ti sheet.[20] In a typical synthesis, Ti sheets (area equal to 2 × 1 cm^2) were chemically polished, treated by sonication in ethanol and cleaned in a 5 wt% of oxalic acid aqueous solution at 100 °C for 2 h, followed by rinsing with deionized water and drying. A cleaned and homogeneous coarse surface of Ti plate was thus obtained. The pretreated Ti sheets were then hydrothermally treated at *j* temperature (*j* = 80 or 100 °C) in a solution made of 15 mL of H_2O_2 (30 wt%) and 15 mL of NaOH (10 M) in a Teflon-lined stainless steel autoclave (with a capacity of 100 mL) for *i* time (*i* = 24, 48 or 72 h). After cooling the autoclave to room temperature, the Ti sheets were rinsed gently with deionized water and dried. A protonation was conducted through two cycles of ion exchange in 50 mL of HCl (0.1 M) for 2 h and followed by rinsing with deionized water and drying at 80 °C for 1 h. Finally, the sheets were calcined at 400 °C for 1 h. The resulting samples were quoted AT-*i*-*j* in the following sections.

Film characterization

The structures of the produced nanostructures were characterized by Grazing Incidence X-ray Diffraction (GIXRD) using a Panalytical Empyrean equipped with a multichannel detector (PIXcel 3D) and Cu-Kα radiation, in the 20–90° range, with a scan step of 0.07° for 5.3 s. A five-axes cradle with motorized movements was used to obtain a perfectly plane position of the sample and a 1/16° slit was installed in the incident path and a collimator plate in the diffracted path to form a parallel beam. For all the analyzed samples, the incidence angle ω is equal to 1°. Their microstructure was analyzed using a Supra40 ZEISS Field Emission Gun Scanning Electron Microscope (FEG-SEM) operating at 2.5 kV through top and cross views. The samples were observed directly on the microscope after a carbon coating in the first case, while they were specifically prepared in the second case. They were typically mounted in cold-setting epoxy resin (EpoFix from Struers) and allowed to cure at least 12 h. The metallographic preparation consisted then of grinding with silicon carbide papers using water as lubricant until a mirror effect is reached. Final polishing was performed with an aluminum oxide suspension on a polishing cloth. Samples were then cleaned and dried using an air gun before to be carbon coated for SEM observations. Observations of isolated nanofibers were also performed by Transmission Electron Microscopy (TEM) using a JEM-100CX-II microscope operating at 100 kV. X-ray photoelectron spectroscopy (XPS) was also performed using a Thermo VG ESCALAB 250 instrument equipped with a micro-focused, monochromatic A1 Kα X-ray source (1486.6 eV) and a magnetic lens. The X-ray spot size was 500 μm (15 kV, 150 W). The spectra were acquired in the constant analyzer energy mode with pass energy of 150 and 40 eV for the general survey and the narrow scans, respectively. Finally, the UV-visible diffuse reflectance spectra of the produced films were recorded on a Perkin Elmer-Lambda 1050 spectrophotometer equipped with a PTFE-coated integration sphere.

Photocatalysis tests

The activity of the produced TiO_2 nanostructures was determined by measuring the decomposition of methylene blue (MB) in aqueous solution under ultraviolet light irradiation for different exposition times. The UV light was obtained using a UV lamp (VL-6.LC at 365 nm) with a power of 12 W, purchased from VILBER-Germany. Typically, 10 mL of MB aqueous solution (10 mg L^{-1}) were placed in a vessel and photocatalyst films (area of 2 × 1 cm^2) were placed into the solution for each test. Prior to each irradiation, the solution was magnetically stirred in the dark for 30 min to promote an adsorption–desorption equilibrium. MB decomposition evaluation was carried out using Carry UV-Visible absorption spectroscopy working in a transmission mode, following the MB absorption peak intensity decrease at *ca.* 660 nm.[23]

Photoelectrocatalysis tests

The photo-response of all the prepared films was evaluated by measuring the photocurrent density J_p, using a scanning potentiostat (Metrohm AUTOLAB PGSTAT12 Instrument). The measurement of the photocurrent density as a function of the applied potential *E* was performed in a standard three-electrode configuration (single-compartment) home-made cell.[22] The potential of each prepared sample (used as a working electrode) was measured using a saturated calomel electrode (SCE) as reference and a Pt wire as counter electrode. A solution of Na_2SO_4 (0.5 M, pH = 7) was used as an electrolyte. The whole cell was purged with argon to remove any dissolved oxygen prior to all experiments. A surface of 0.7 × 1.0 cm^2 was illumined on each sample by a 150 W Xenon lamp (ORIEL instruments), to mimic solar light.

Results and discussion

Phase analysis

XRD was first used to identify and determine the phase structure of all produced samples. Fig. 1 displays the recorded XRD patterns.

They match very well with that of pure TiO_2 and Ti phases. The diffraction peaks are fully indexed in the tetragonal anatase structure (ICDD no. 00-021-1272) and the hexagonal titanium one (ICDD no. 00-044-1294) for the films produced at 80 °C (Fig. 1a) while a supplementary contribution is identified in those produced at 100 °C. For these samples specifically, very small peaks related to the TiO_2 (b) phase (ICDD no. 00-046-

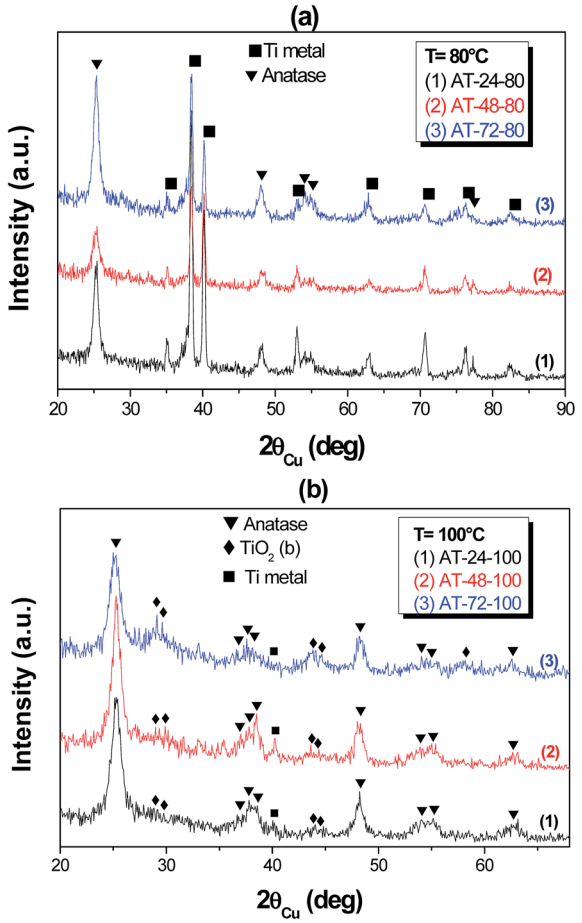

Fig. 1 XRD patterns of the synthesized TiO_2 nanostructures (a) at 80 °C and (b) at 100 °C for different heating times.

1238), a less common monoclinic form of titania, are identified (Fig. 1b). Note the Ti peak's intensity gradually decreases by increasing the hydrothermal time treatment, suggesting an increasing titania shell thickness in the corresponding films. This result is in agreement with that obtained by SEM observations (see Fig. 2). Indeed, the top and cross section views of all the produced TiO_2/Ti nanostructures, given in Fig. 2, illustrate the evolution of their microstructure as a function of their hydrothermal treatment conditions, namely the reaction time and temperature. Obviously, a homogeneous macro and micro porous surface structure is observed. The recorded micrographs show highly connected, more or less long and thin TiO_2 nanofibers (NFs) supported on the Ti sheets. Note that, NFs appear to be composed of sub-nanofibers of less than 10 nm in diameter. Their density on the metal substrate increases when the reaction temperature increases and the samples obtained at 100 °C are denser than those obtained at 80 °C. Moreover, by increasing the reaction temperature, NFs become thinner and longer, exhibiting in samples AT-48-100 and AT-72-100 a typical feature of nanowires (Fig. 2h and i). Finally, as expected, the volume fraction of corroded Ti metal during hydrothermal treatment increases with the reaction time increase, leading to more and more thick titania layer on the supporting Ti sheets (see Fig. 2d–f and j–l), which is itself constituted by more and more thin and long TiO_2 NFs (see Fig. 2a–c and g–i). Clearly, the extension of the synthesis time affects the morphology of the nanostructures, and these changes are much more spectacular when they are prepared at 100 °C instead of 80 °C.

These results are also illustrated by the TEM and HRTEM captured images for two representative samples of the studied series, namely AT-24-80 and AT-72-100 (Fig. 3). Both micrographs confirm the evolution of the morphology of the produced TiO_2 nanostructures and show thinner and longer NFs by increasing reaction time and temperature. These morphology changes are crucial and will could greatly affect the photocatalytic and photoelectrocatalytic behavior of the studied materials.[13]

To confirm the TiO_2 nature of the produced NFs, the chemical surface composition of all the prepared samples was examined by X-ray photoelectron spectroscopy. The recorded survey spectra of all the samples show mainly the binding energies of C 1s, Ti 2p and O 1s, at about 285, 458 and 530 eV respectively. The spectra of two representative samples, namely AT-24-80 and AT-72-100, are given in Fig. 4. Note that peak positions were calibrated against the C 1s adventitious carbon main peak component C–C/C–H set at 285 eV. High resolution spectra were also recorded in order to get new insights about the electronic states of the various elements. They are given for C 1s, Ti 2p and O 1s peaks in Fig. 5 for the same representative samples. The results of C 1s and O 1s signal decomposition are detailed in the ESI.† An attentive observation of the C 1s signal shows that it is in fact composed by three peaks with binding energies of 285.0 eV, 286.5 eV and 289.0 eV, respectively. The first and the strongest one is effectively assigned to C–H and/or C–C bonds of adventitious carbon but the less intense second and third ones are assigned to C–O and C=O bonds of carbonates, respectively.[24] A rapid overview of the relevant literature shows that the peak at 289 eV might be assigned to a carbon doping of the TiO_2 lattice.[25,26] This doping may concern Ti and/or oxygen substitution. The former is unlikely in TiO_2 because of the large mismatch in both electronegativity and atomic radius of titanium and carbon. The latter is more probable through Ti–O–C bonds.

Doping of TiO_2 by carbon was already observed and largely discussed in several previous works.[29] Thus it has been shown that carbon substituting oxygen can form carbonate like bonds ($O{=}C(-O)_2$).[26] Anyway, these last carbon species should introduce doping states into the wide band-gap TiO_2 semiconductor, leading to an increase of its visible light absorption[25,26] and then to its sunlight photo-conversion yield. Moreover, the atomic percentage of carbonate (represented by C 1s A and B components in Fig. 5) in AT-24-80 is more by two folds than in AT-72-100 (Table 1). It is systematically higher in all the sample series obtained at 80 °C in comparison to those prepared at 100 °C. This result must be underlined because it clearly suggests that the former absorb in a wider light wavelength range.

Surprisingly, samples prepared in almost the same conditions than AT-24-80 ones, namely an hydrothermal treatment at 80 °C during 24 h of a Ti sheet, did not evidence such carbon contamination,[22] underlining once again how much the

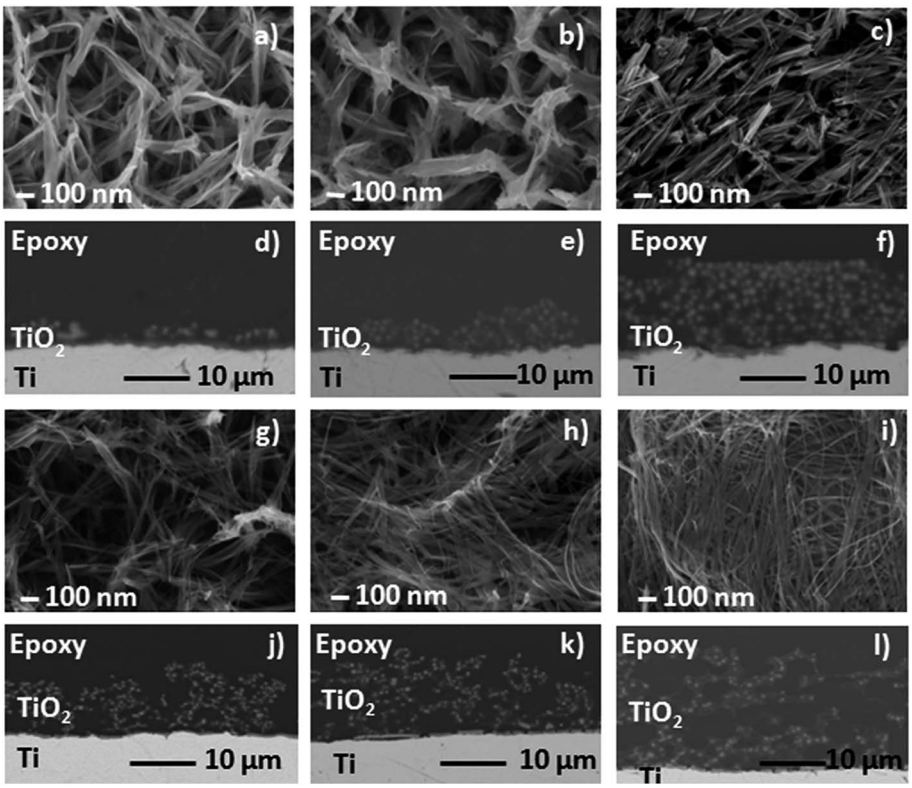

Fig. 2 Top (a–c) and cross section (d–f) views of the TiO_2/Ti nanostructures synthesized by hydrothermal oxidation of Ti sheets at 80 °C for 24, 48 and 72 h, respectively, and their analogous (g–i) and (j–l) for the nanostructures obtained at 100 °C for the same heating times.

experimental synthesis conditions may drastically affect the properties of the produced TiO_2/Ti nanostructures. Indeed, by changing the purity of the Ti sheet (99.7% *versus* 99.6% in the previous and the present works, respectively) and the autoclave capacity (30 mL *versus* 100 mL in the previous and the present works, respectively), we introduced a carbon contamination contributing in the visible light absorption enhancement in the last sample series. Interestingly, by increasing the heating temperature from 80 to 100 °C, this carbon contamination can be significantly reduced as established here by the XPS characterization of the AT-72-100 samples.

Contrary to carbon content which is higher in AT-24-80, the oxygen content in AT-72-100 is higher than that in AT-24-80 sample. The O 1s spectrum can be decomposed in three peaks with binding energies of 529.3, 531.0 and 532.5 eV for AT-24-80 sample and 530.2, 531.6 and 532.8 eV for AT-72-100 sample (see Fig. SI 1 in the ESI†). The first peak for both samples is assigned to oxygen in TiO_2 while the second and the third ones are attributed to oxygen in carbonates C=O and C–O, respectively. Moreover, a shift, in the same direction, towards higher binding energies of both Ti 2p and O 1s is observed for AT-72-100 (Fig. 5). This shift may be due to a Fermi level displacement (in AT-72-100 with respect of AT-24-80) toward the middle of the band gap which causes apparent rigid bending energy shift in the same direction irrespective of the atomic

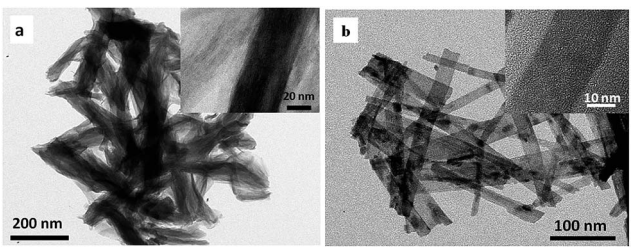

Fig. 3 TEM and HRTEM images (in the inset) of representative TiO_2 NFs synthesized at 80 °C for 24 h (a) and at 100 °C for 72 h (b).

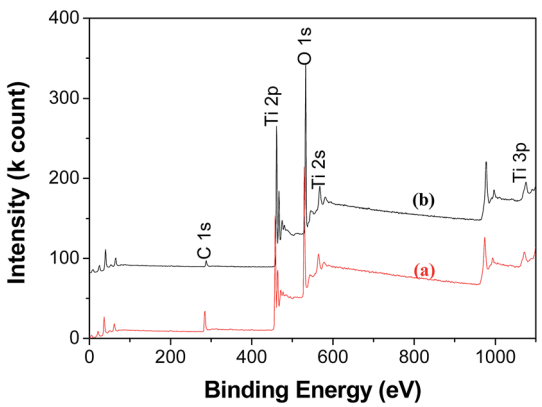

Fig. 4 Low resolution XPS spectra of TiO_2/Ti nanostructures synthesized at 80 °C for 24 h (a) and at 100 °C for 72 h (b).

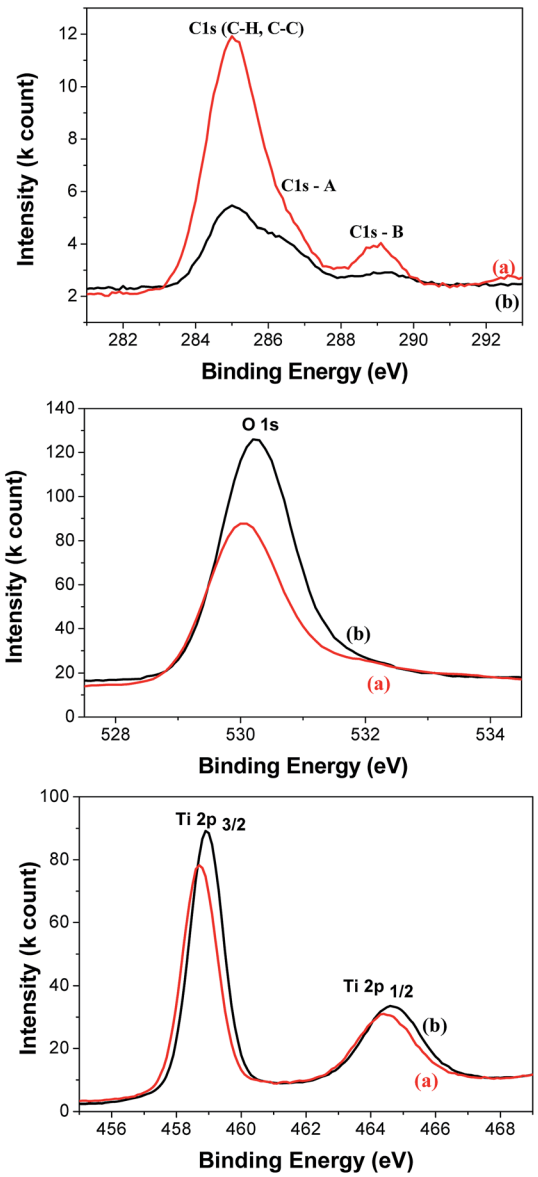

Fig. 5 High resolution XPS spectra of the C 1s, O 1s and Ti 2p signals recorded on the TiO_2/Ti nanostructures synthesized at 80 °C for 24 h (a) and at 100 °C for 72 h (b).

species involved.[27] This indicates once again that AT-72-100 sample is less doped than AT-24-80 one since its Fermi level is far below the conduction band. More generally, the films produced at 100 °C are less doped than those obtained at 80 °C.

At the end of this series of characterizations, UV-visible diffuse reflectance spectroscopy was employed. The recorded absorption spectra are given in Fig. 6 for all the produced samples.

The titanium dioxide absorbs ultraviolet mainly between 250 and 350 nm. Between 350 and 400 nm, the absorption decreases rapidly and becomes stable and almost negligible in the case of samples prepared at 100 °C, while it increases again to form a large band in the visible range in the nanostructure synthesized at 80 °C. This discrepancy between the two AT-*i*-100 and AT-*i*-80 series agrees very well with the XPS analysis results and

Table 1 Surface chemical composition of two representative TiO_2/Ti nanostructures of the studied series as inferred from XPS analysis, namely AT-24-80 and AT-72-100[a]

	Element	Energy (eV)	At%
AT-24-80	O 1s	530.1	50.0*
	C 1s	285.0	20.0
	C 1s A	286.5	4.9
	C 1s B	289.0	2.8
	Ti 2p	458.7	22.3*
AT-72-100	O 1s	530.3	66.5**
	C 1s	285.0	5.2
	C 1s A	286.5	2.9
	C 1s B	289.1	0.9
	Ti 2p	458.9	24.5**

[a] *O/Ti = 2.2, **O/Ti = 2.7.

confirms the suspected higher carbon doping content in the latter compared to the former. Carbon doping contribute to the enhancement of the visible light absorption of the produced films and may contribute to the enhancement of their photocatalytic and photoelectrocatalytic properties. By comparing the spectra of the samples produced at a given temperature for

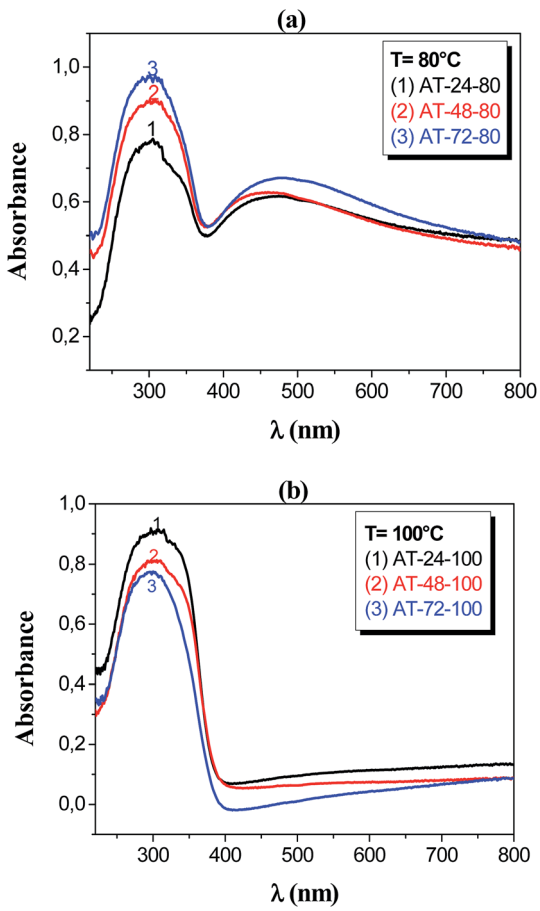

Fig. 6 UV-Visible diffuse reflectance spectra of TiO_2/Ti nanostructures synthesized at 80 °C (a) and 100 °C (b) for different reaction times.

different reaction times, the absorbance varies monotonously when the reaction time is prolonged from 24 to 72 h. It increases with lengthening synthesis time in the case of the samples prepared at 80 °C (Fig. 6a) in relation with the increase of their titania content and probably the increase of their porosity as well (see Fig. 2d–f).

By contrast, it decreases in the case of samples prepared at 100 °C (Fig. 6b) and the maximum of absorbance in the UV region is shifted toward lower wavelengths, indicating an increase of the band-gap for this series of semiconductors with time of hydrothermal treatment. We believe that these optical changes are related to the reduction of NF diameter as evidenced by SEM and TEM analysis and also to the elimination of TiO_2 lattice defects as suggested by XPS investigation. The absorbance reduction *versus* time is also plausible with a progressive densification of the TiO_2 1D nanostructures, and then with a less porous and roughness surface.

Photocatalytic properties

The photocatalytic degradation of MB as a pollutant model by the prepared TiO_2/Ti films was evaluated by following the absorbance of its characteristic band, centered at about 660 nm, in the optical spectra of a series of MB aqueous solutions irradiated by UV light for different times. Fig. 7 gives these spectra for an exposure time of 22 h in presence of the various catalyst films. Clearly, the AT-24-80 and AT-72-100 samples present the highest intrinsic activity as evidenced by the considerable decrease of MB absorbance, in relation with MB concentration decrease (see the variation of the relative MB concentration $C(t)/C(t=0)$ as a function of UV exposition time t given in the ESI†).

Using these data, the photodegradation conversion rate, τ, was calculated for each catalyst:

$$\tau = \frac{C(t=0) - C(t)}{C(t=0)} \times 100 \quad (1)$$

where $C(t=0)$ represents the initial MB concentration and $C(t)$ its concentration after a t irradiation time. The variation of the calculated conversion rate as a function of UV exposition time was then plotted for all the produced catalysts in Fig. 8 and its final value along for an irradiation time of 24 h is given in Table 2.

Significantly, the conversion rate depends on the morphology of the produced TiO_2/Ti nanostructures which in turn depends on the hydrothermal treatment conditions, namely the heating time and temperature. It is obvious in Fig. 8 that the degradation is faster with AT-24-80 catalyst after 3 h of irradiation. As against by contrast, it is more important with AT-72-100 one after 6 h of irradiation. But after about 24 h of UV exposition, the best conversion rate is obtained using specifically this catalyst, with a value of 86%. This sample exhibits the

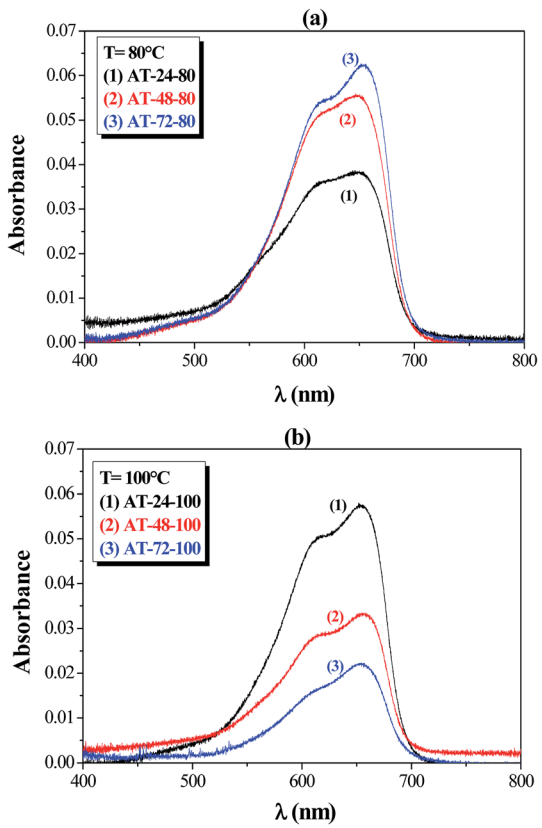

Fig. 7 Variation of the dye absorption spectra after a UV radiation exposition of 22 h in presence of TiO_2/Ti films produced at 80 °C (a) and 100 °C (b) for different heating times.

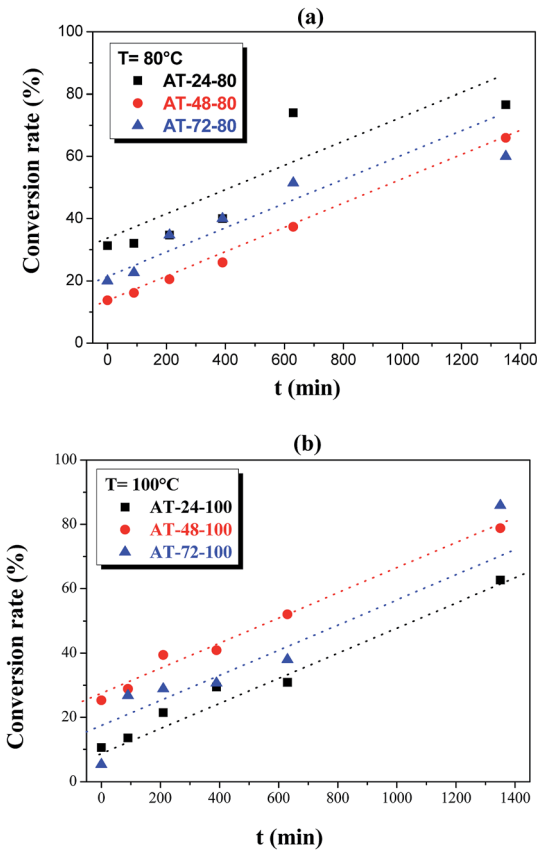

Fig. 8 Temporal evolution of the MB conversion during photodegradation by TiO_2/Ti films produced at 80 (a) and 100 °C (b) for different heating times (dashed lines are guide for eyes).

Table 2 Conversion rate value of MB for an irradiation time of 24 h

Sample	AT-24-80	AT-48-80	AT-72-80	AT-24-100	AT-48-100	AT-72-100
τ (%)	79	66	60	63	76	86

finest titania microstructure. It is constituted by a dense array of long and thin nanowires supported on Ti sheets. Thanks to its advantageous morphology and structure, it clearly offers the best photocatalytic capabilities for efficient, rapid and eco-friendly waste water depollution.

Photoelectrochemical properties

PEC performances of all the produced TiO_2/Ti films were investigated by cyclic voltammetry under dark and illumination (Fig. 9). All the photoanodes show negligible current under dark conditions. However, the dark currents of the AT-*i*-100 samples are relatively higher indicating that these samples could present lower bulk and/or interfacial resistance. Under illumination, the samples produced at 100 °C exhibit more intense photocurrent (Fig. 9) despite their poor absorption in the visible light region. This may be due to their good crystallinity (Fig. 3b), fine structure and porosity (Fig. 2g–i). From all the studied sample series, the sample that was treated during 48 h at 100 °C (AT-48-100) seems to be the best for PEC applications, since it presents the highest photocurrent and the lowest open circuit voltage under illumination. The decrease in open circuit voltage (onset potential) under light where the photocurrent set up may be due to the large diffusion or the low recombination of the generated carriers[28] as a result of good crystallinity and appropriate porosity. Under illumination, the photocurrent for AT-48-100 (Fig. 9b) is generated at working electrode potentials as low as −0.22 V *vs.* SCE, giving the flat band potential (E_{fb}) at the TiO_2/electrolyte contact (the flat band potential represents the apparent Fermi level of the semiconductor in equilibrium with the redox couple). The photocurrent rises as the anode potential increases, reflecting increased charge carrier separation efficiency.[28]

Furthermore, the short-circuit current also increases significantly with treatment time in the case of AT-*i*-100 series. It is worth noting that the photocurrent is formed mainly by diffusion of the photogenerated electrons to the back contact, while the photo-induced holes are taken up by the acceptor holes in the electrolyte. As shown in Fig. 9a, the photocurrent is relatively low and the onset potential is large in all the samples of AT-*i*-80 series which show lower crystallinity and larger porosity.

We also measured the transient photocurrent in 0.5 M Na_2SO_4 electrolyte, under intermittent illumination with and without bias potential *versus* SCE (namely, 0.5 V), for several

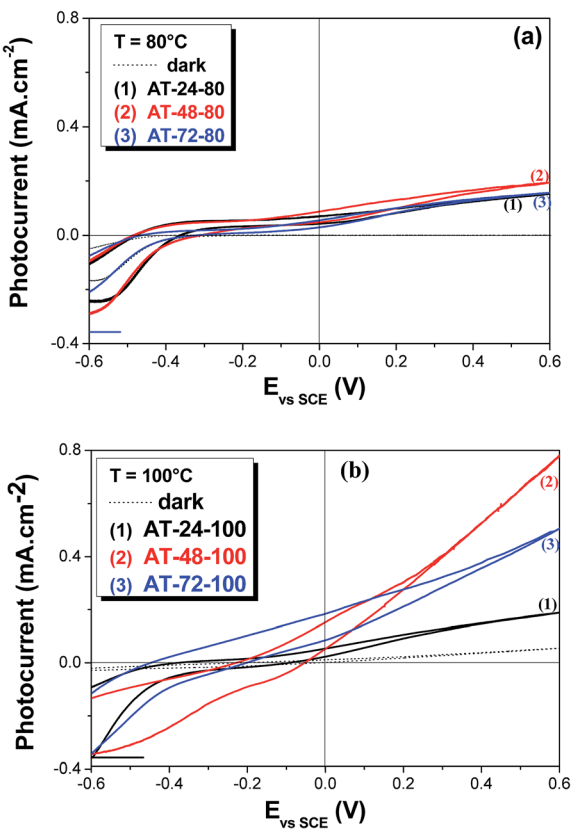

Fig. 9 Photocurrent *vs.* potential curves plotted under illumination for TiO_2/Ti films produced at 80 (a) and 100 °C (b) for different heating times. The potential scan rate was fixed to 10 mV s^{-1}.

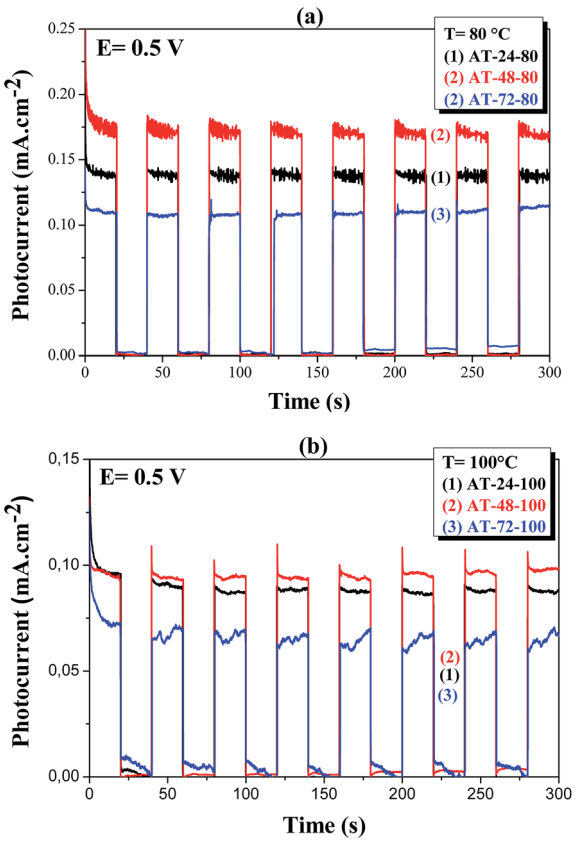

Fig. 10 Photocurrent responses in the Na_2SO_4 aqueous solution (0.5 M, pH = 7) of TiO_2/Ti films produced at 80 (a) and 100 °C (b) for different heating times, with a bias E = 0.5 V *vs.* SCE.

cycles, to appreciate the reproducibility of the photo-response of our catalyst series (Fig. 10).

All the photoanodes led to an instantaneous change in current upon illumination. The current retracted to its original values almost instantaneously as well once the illumination was switched off. This trend was repeated for every on–off cycle, indicating that the anodes were corrosion resistant under photo-illumination.

Finally, the microstructure and the surface chemical composition of the used films for MB photocatalytic degradation or photo-electrocatalytic water oxidation test cycles were checked after use (see ESI†). They appear to be almost unchanged after prolonged wastewater and/or electrolyte contact time underlining once again the robustness of the material-processing route and how it is efficient to build relatively stable catalysts for the desired applications.

Conclusion

A series of TiO_2 nanofibers supported on Ti sheets was prepared by hydrothermal oxidative treatment of metal plates at 80 and 100 °C, respectively, for different heating times, namely 24, 48 and 72 h. Structural and microstructural investigations shows that acting on these two synthesis parameters, namely the reaction time and temperature, it is possible to tune the morphology of the nanofibers from thick and short nanorods at short and low heating time and temperature, respectively, to thin and long nanowires at long and high heating time and temperature, respectively. The produced titania appears to be mainly constituted by anatase phase. The optimum conditions of hydrothermal treatment for the photocurrent enhancement in the present work are 100 °C and 48 h. This study provides information on the efficiency of the photocatalysts and their PEC properties which allowed choosing the best system for water splitting (in progress).

Acknowledgements

This work was supported by the Algerian and French Scientific Research cooperation (PROFAS program). The authors are indebted to Dr P. Beaunier from Pierre and Marie Curie University (Paris 6) for her technical support on TEM-HRTEM facilities.

References

1 (*a*) K. Madhusudan Reddy, S. V. Manorama and A. Ramachandra Reddy, Bandgap studies on anatase titanium dioxide nanoparticles, *Mater. Chem. Phys.*, 2002, **78**(1), 239–245; (*b*) X. Chen and S. S. Mao, Titanium dioxide nanomaterials: synthesis, properties, modifications, and applications, *Chem. Rev.*, 2007, **107**(7), 2891–2959.

2 (*a*) T. L. Thompson and J. T. Yates Jr, Surface science studies of of the Photoactivation of TiO_2: New photochemical processes, *Chem. Rev.*, 2006, **106**(10), 4428–4453; (*b*) M. R. Hoffmann, S. T. Martin, W. Y. Choi and D. W. Bahnemann, Environmental applications of semiconductor potocatalysis, *Chem. Rev.*, 1995, **95**(1), 69–96; (*c*) A. Fujishima, X. Zhang and D. A. Tryk, TiO_2 photocatalysis and related surface phenomena, *Surf. Sci. Rep.*, 2008, **63**(12), 515–582; (*d*) D. Ravelli, D. Dondi, M. Fagnonia and A. Albini, Photocatalysis: A multi-faceted concept for green chemistry, *Chem. Soc. Rev.*, 2009, **38**(7), 1999–2011.

3 L. Jing, S. Li, S. Song, L. Xue and H. Fu, Investigation on the electron transfer between anatase and rutile in nano-sized TiO_2 by means of surface photovoltage technique and its effects on the photocatalytic activity, *Sol. Energy Mater. Sol. Cells*, 2008, **92**(9), 1030–1036.

4 (*a*) G. Wang, Hydrothermal synthesis and photocatalytic activity of nanocrystalline TiO_2 powders in ethanol–water mixed solutions, *J. Mol. Catal. A: Chem.*, 2007, **274**(1–2), 185–191; (*b*) R. Sahni and K. Madhusudan Reddy, Influence parameters on the synthesis of nano-titania by sol-gel route, *Mater. Sci. Eng., A*, 2007, **452–453**, 758–762.

5 M. Francisco and V. Mastelaro, Inhibition of the anatase-rutile phase transformation with addition of CeO_2 to CuO–TiO_2 system: Raman spectroscopy, X-ray diffraction and textural studies, *Chem. Mater.*, 2002, **14**, 2514–2518.

6 I. Paramasivam, H. Jha, N. Liu and P. Schmuki, A review of photocatalysis using self-organized TiO_2 nanotubes and other ordered oxide nanostructures, *Small*, 2012, **8**(30), 3073–3103.

7 Z. Miao, D. Xu, J. Quyang, G. Guo, X. Zhao and Y. Tang, Electrochemically induced sol-gel preparation of single-crystalline TiO_2 nanowires, *Nano Lett.*, 2002, **2**(7), 717–720.

8 Y. Lei, L. D. Zang, G. W. Meng, G. H. Li, X. Y. Zhang, C. H. Liang, W. Chen and S. X. Wang, Preparation and photoluminescence of highly ordered TiO_2 nanowire arrays, *Appl. Phys. Lett.*, 2001, **78**(8), 1125–1127.

9 M. Gratzel, Photoelectrochemical cells, *Nature*, 2001, **414**(6861), 338–344.

10 A. Linsebigler, G. Lu and J. T. Yates Jr, hotocatalysis on TiO_2 surfaces: Principles, mechanisms and selected results, *Chem. Rev.*, 1995, **95**(3), 735–758.

11 G. Mor, K. Shankar, M. Paulose, O. K. Varghese and C. A. Grimes, Use of highly-ordered TiO_2 nanotube arrays in dye-sensitized solar cells, *Nano Lett.*, 2006, **6**(2), 215–218.

12 Z. Y. Yuan, W. Zhou and B. L. Su, Hierarchical interlinked structure of titanium oxide nanofibers, *Chem. Commun.*, 2002, 1202–1203.

13 Y. Lai, J. Gong and C. Lin, Self-organized TiO_2 nanotube arrays with uniform platinum nanoparticles for highly efficient water splitting, *Int. J. Hydrogen Energy*, 2012, **37**(8), 6438–6446.

14 S. Chaguetmi, F. Mammeri, S. Nowak, H. Lecoq, P. Decorse, C. Costentin, S. Achour and S. Ammar, Synergetic effect of CdS quantum dots and TiO_2 nanofibers for photo-electrochemical hydrogen generation, *J. Nanopart. Res.*, 2013, **15**(12), 2140–2146.

15 O. A. Ileperuma, K. Tennakone and W. D. D. P. Dissanayake, Photocatalytic behavior of metal doped titanium dioxide:

Studies on the Photochemical Synthesis of Ammonia on Mg/TiO_2 Catalyst Systems, *Appl. Catal.*, 1990, **62**(1), L1–L5.

16 R. Asahi, T. Morikawa and T. Ohwaki, Visible-Light Photocatalysis in Nitrogen-Doped Titanium Oxides, *Science*, 2001, **293**(5528), 269–271.

17 T. Kasuga, M. Hiramatsu, A. Hoso, T. Sekino and K. Niihara, Titania Nanotubes Prepared by Chemical Processing, *Adv. Mater.*, 1999, **11**(15), 1307–1311.

18 A. R. Armstrong, G. Armstrong, G. Canales and P. G. Bruce, TiO_2-B Nanowires, *Angew. Chem., Int. Ed.*, 2004, **43**(17), 2286–2288.

19 R. Yoshida, Y. Suzuki and S. Yoshikawa, Syntheses of TiO_2(B) nanowires and TiO_2 anatase nanowires by hydrothermal and post-heat treatments, *J. Solid State Chem.*, 2005, **178**(7), 2179–2185.

20 Y. Wu, M. Long, W. Cai, S. Dai, C. Chen, D. Wu and J. Bai, Preparation of photocatalytic anatase nanowire films by *in situ* oxidation of titanium plate, *Nanotechnology*, 2009, **20**(18), 185703.1–185503.8.

21 J. Ng, J. Hong Pan and D. Delai Sun, Hierarchical assembly of anatase nanowhiskers and evaluation of their photocatalytic efficiency in comparison to various one-dimensional TiO_2 nanostructures, *J. Mater. Chem.*, 2011, **21**(32), 11844–11853.

22 S. Chaguetmi, F. Mammeri, M. Gaceur, S. Nowak, P. Decorse, H. Lecoq, A. Slimane, R. Chtourou and S. Ammar, Photocatalytic activity of TiO_2 nanofibers sensitized with ZnS quantum dots, *RSC Adv.*, 2013, **3**(8), 2572–2580.

23 J. Ben Naceur, M. Gaidi, F. Bousbih, R. Mechiakh and R. Chtourou, Annealing effects on microstructural and optical properties of Nanostructured-TiO_2 thin films prepared by sol-gel technique, *Curr. Appl. Phys.*, 2012, **12**(2), 422–428.

24 B. Liu, L. M. Liu, X. F. Lang, H. Y. Wang, X. W. Lou and E. S. Aydil, Doping high-surface-area mesoporous TiO_2 microspheres with carbonate for visible light hydrogen production, *Energy Environ. Sci.*, 2014, **7**(8), 2592–2597.

25 Z. He, J. Xiao, F. Xia, K. Kajiyoshi, C. Samart and H. Zhang, Enhanced solar water-splitting performance of TiO_2 nanotube arrays by annealing and quenching, *Appl. Surf. Sci.*, 2014, **313**, 633–639.

26 H. Jensen, A. Soloviev, Z. Li and E. G. Søgaard, XPS and FTIR investigation of the surface properties of different prepared titania nano-powders, *Appl. Surf. Sci.*, 2005, **246**(1–3), 239–249.

27 A. Achour, K. Ait Aissa, M. Mbarek, K. El Hadj, N. Ouldhamadouche, N. Barreau, L. Le Brizoual and M. A. Djouadi, Enhancement of near-band edge photoluminescence of ZnO film buffered with TiN, *Thin Solid Films*, 2013, **538**, 71–77.

28 N. Sobti, A. Bensouici, F. Coloma, C. Untiedt and S. Achour, Structural & photo-electrochemical properties of porous TiO_2 nanofibers decorated with Fe_2O_3 by sol-flame, *J. Nanopart. Res.*, 2014, **16**(8), 2577–2582.

29 (*a*) Y. Zhao, Y. Li, C. W. Wang, J. Wang, X. Q. Wang, Z. W. Pan, C. Dong and F. Zhou, Carbon-doped anatase TiO_2 nanotube array/glass and its enhanced photocatalytic activity under solar light, *Solid State Sci.*, 2013, **15**, 53–59; (*b*) Y. Park, W. Kim, H. Park, T. Tachikawa, T. Majima and W. Choi, Carbon-doped TiO_2 photocatalyst synthesized without using an external carbon precursor and the visible light activity, *Appl. Catal., B*, 2009, **91**, 55–361; (*c*) X. Wang, S. Meng, X. Zhang, H. Wang, W. Zhong and Q. Du, Multi-type carbon doping of TiO_2 photocatalyst, *Chem. Phys. Lett.*, 2007, **444**, 292–296; (*d*) J. H. Park, S. Kim and A. J. Bard, Novel Carbon-Doped TiO_2 Nanotube Arrays with High Aspect Ratios for Efficient Solar Water Splitting, *Nano Lett.*, 2006, **6**, 24–28; (*e*) Y. Li, D. S. Hwang, N. H. Lee and S. J. Kim, Synthesis and characterization of carbon-doped titania as an artificial solar light sensitive photocatalyst, *Chem. Phys. Lett.*, 2005, **404**, 25–29.